



Smart sensor network for power quality monitoring in electrical installations



Luis Morales-Velazquez^a, Rene de Jesus Romero-Troncoso^b, Gilberto Herrera-Ruiz^a, Daniel Morinigo-Sotelo^c, Roque Alfredo Osornio-Rios^{a,*}

^a CA Mecatronica, Facultad de Ingenieria, Universidad Autonoma de Queretaro, Campus San Juan del Rio, Rio Moctezuma 249, Colonia San Cayetano, 76807 San Juan del Rio, QRO, Mexico

^b CA Telematica, DICIS, Universidad de Guanajuato, Carr. Salamanca-Valle km 3.5+1.8, Palo Blanco, 36885 Salamanca, GTO, Mexico

^c Department of Electrical Engineering, University of Valladolid (UVa), 47011 Valladolid, Spain

ARTICLE INFO

Article history:

Received 22 December 2016

Received in revised form 5 February 2017

Accepted 17 February 2017

Available online 20 February 2017

Keywords:

Smart sensor network

Power quality

FPGA

Smart grid

ABSTRACT

Smart meters are one of the basic components of the future smart grid, they allow remotely monitoring each point in the grid in order to know in real-time the performance of the system and to detect potential failures. In this paper, a smart sensor network is introduced and the most important features are presented in three different scenarios: a residential home, an industrial installation, and a public building. The proposed system demonstrates its capabilities of in situ real-time processing and big-data off-line network processing. The suggested smart meter is based on field programmable gate array (FPGA) technology that allows a reconfigurable architecture, which lets the user to select the proper processing modules according to their application. The developed smart sensor network calculates standard figures such as effective values, power factor, and total harmonic distortion; in addition, it detects power quality disturbances such as dips, swells, or interruptions. Moreover, the smart sensor network can continuously detect events to identify certain kind of appliances or industrial equipment such as: fans, lighting, microwave ovens, refrigerators, among others; it is a powerful tool to analyze an entire building in a non-intrusive load monitoring approach.

© 2017 Elsevier Ltd. All rights reserved.

1. Introduction

Power quality (PQ) monitoring is essential in the smart grid paradigm [1], where smart meters are one of the basic elements in the grid to measure power consumption and to detect power quality disturbances (PQD). Smart sensors are a device concept that includes a sensing element, signal processing capabilities, communications, and integration [2]. Furthermore, smart meters additionally require data storage and synchronization to operate in a network environment extending the smart sensor concept to a smart sensor network approach [3]. On the other hand, electrical installations are mostly instrumented with measurement equipment at the customer point, basically for billing purposes, not for monitoring. Additionally, distribution centrals in electrical systems carry out energy measurement to reduce PQD. However, after this distribution point, the instrumentation for PQ monitoring in the

electrical installation is scarce or nonexistent. Moreover, PQ monitoring equipment is costly and is not designed for continuous monitoring. Since PQ is an important requirement in smart grids, international standards have been developed to classify electrical disturbances [4,5] that affect the grid or the user.

Power management policies such as PQ and PQD monitoring, smart grid interaction, and load monitoring will be common in the next years; where residential and public buildings, as well as industrial facilities, would use these policies to reduce its energy consumption and cost, increasing their sustainability. The PQ definition stated by the standards IEEE-1159 [4] and EN-50160 [5] sets the methodology and the threshold values that define an electrical disturbance such as an over voltage (swell), under voltage (sag or dip), fluctuation, harmonic distortion, etc. The electrical installation inside buildings is subject to additional regulations depending on their functions; the IEC-60364 standard defines such requirements for a wide variety of buildings [6–8]. Thus, to monitor electrical installations at a building scale a smart sensor network is a necessity to save energy and to detect potential failures at an early stage. Despite the standards, load interactions have unknown effects over appliances for home or industry; thus, it is

* Corresponding author.

E-mail addresses: lmorales@hspdigital.org (L. Morales-Velazquez), troncoso@hspdigital.org (R.J. Romero-Troncoso), daniel.morinigo@eii.uva.es (D. Morinigo-Sotelo), raoosornio@hspdigital.org (R.A. Osornio-Rios).

important to study their sources, effects and propagation behavior in order to develop protections for sensitive apparatus, e.g. electromedical equipment in hospitals. In the state-of-art literature, the PQ subject is centered on techniques for the classification and the detection of PQD [9] used in large distribution systems [10]. For instance, Prakash et al. [11] proposed an S-transform methodology to detect PQD, having better results than the wavelet transform approach. Camarena et al. [12] proposed a method based on empirical mode decomposition to detect fundamental components of the power signal in order to reduce the computational effort. In addition, Prakash and Gafoor [13] made a review of a number of techniques to improve PQ in distribution systems. Furthermore, with the implementation of the smart grid where buildings become sinks and sources of energy, power management faces new challenges with great potential benefits [14]. Therefore, some power management systems have been developed [15] to deal with those new challenges; e.g., Cerqueira et al. [16] presented a study that highlights the problem of the integration of photovoltaic generators to the grid, determining which of these facilities are economically viable. Even though, current PQ and smart grid research are focused onto generation, transmission, and distribution, it can also be applied to building scale, with a microgrid approach [17]. Additionally, some research has been carried out to analyze the power consumption in public buildings. Christiansen et al. [18] made a study of power consumption in hospital laboratories to estimate the power consumption of each instrument, but there is no concern neither in PQD nor system performance. The current commercially available smart meter equipment is mostly used to billing; but since the smart grid is expanding, the metering equipment needs to be smarter also [19] to include new features such as PQD detection. On this way, Jaradat et al. [1] introduced a smart sensor network capable of managing big-data in smart grids, proposing recommendations and practices to be used on the future smart grid; yet, this work discusses the problem in general terms and the authors do not test their proposal in a real system. Consequently, the design of smart sensor networks for the smart grid must take into account the customer and the grid necessities in order to accomplish the expected performance.

The application of smart meter networks to a smart grid [20] is known as advanced metering infrastructure (AMI), which introduces additional restrictions such as security and remote control [21]. Furthermore, the original equipment manufacturers (OEM) that produce measurement equipment like PQ analyzers, e.g.: Fluke-435 [22], Circutor-QNA500 [23], and Hioki-PW3198 [24], do not satisfy the AMI requirements. Although these commercial instruments are designed to comply with the current international standards, they are not designed to interact with each other neither to detect nor quantify all PQD for the individual appliance consumption. In this way, an open smart sensor network platform is required to implement detailed PQ analysis to accurately measure general power consumption but also at the appliance level to detect events and its propagation on the microgrid. Thus, Klis and Chatzi [25] and Noriega-Linares and Navarro-Ruiz [26] discusses those features required in an instrument that integrates sensors, embedded data processing, massive data storage, wireless communications, and flexible architecture. Usually, devices to perform embedded data processing are the digital signal processors (DSP) and the field programmable gate arrays (FPGA) due to their inherent processing power. For data storage an SD memory card is the widespread option. Meanwhile, wireless communication is essential because the smart sensor networks must have an easy installation and a low cost; thus, a wired network is unviable. It is expected that the smart meter be very flexible in order to be installed in a wide variety of facilities such as industries, public buildings, or residential homes. In addition, an non-intrusive load

monitoring (NIM) approach based on acoustic sensors [27,28], infrared imaging [29], current clamps [30], among other no contact sensors are preferred in order to not to disturb the monitored system.

The contribution of this work is the development of an open-architecture smart sensor network, based on FPGA technology, which is able to continuously monitor PQ in industrial facilities, public buildings, and residential homes. The developed system is capable of acquiring voltage and current signals at a high sampling rate with in a NILM scheme. The smart sensor network is effective to process and fully record voltage and current signals during a long span. The integrated processing capabilities include the estimation of several PQ indexes, the identification of PQD, detect connection and disconnection events, being able to integrate further algorithms to classify, correlate, and isolate particular events. The smart sensor network is also capable to locate events occurring in a synchronized way at several points of the electrical installation. This capability allows the correlation of events, finding interactions between disturbances in order to advance in the construction of an AMI. In addition, the FPGA approach, based on soft-cores, leads it to a high reconfigurability and flexibility of the embedded processing.

The remainder of this paper is organized as follows. In Section 2, a theoretical background is presented to state the embedded algorithms for real-time processing. In Section 3, the proposed system architecture of the smart sensor network is defined. Section 4 presents three application scenarios: a residential home, an industrial installation, and a public hospital. Section 5, covers the experimental setup for all test scenarios. Section 6, discusses the obtained results. Finally, in Section 7, conclusions are stated from the obtained results.

2. Theoretical background

Power quality as defined by the international standards [4,5] is seen as the fitness of the voltage waveform to a purely sinusoidal waveform. Any distortion to the ideal sinusoidal waveform is considered a disturbance; however, the standards set the threshold values to consider a particular distortion as a PQD within a voltage range. For instance, Table 1 shows thresholds based on EN-50160 [5] for an over voltage (swell), an under voltage (dip or sag), an interruption (outage), and total harmonic distortion (THD) for harmonics and interharmonics.

Whereas PQ is defined for the voltage waveform of the fundamental frequency, the first three indexes of Table 1 are based on the effective voltage defined as the root mean square (RMS) using

$$V_{\text{RMS}} = \sqrt{\frac{1}{N-1} \sum_{j=0}^{N-1} v_j^2}, \quad (1)$$

where V_{RMS} represents the effective voltage value, N represents the number of samples, and v_j the j -th sample in the voltage signal. The effective current (I_{RMS}) value is calculated in an analogous form as presented in (1).

Table 1

Example of PQD index threshold levels according to the EN-50160 standard.

PQD index	Duration	Threshold
Dip/Sag	>0.5 cycles	0.1–0.9 p.u.
Swell	>0.5 cycles	1.1–1.8 p.u.
Outage	>0.5 cycles	<0.1 p.u.
Harmonic	–	THD < 8%
Interharmonic	–	

In industrial buildings an important index is the power factor (PF) defined as the ratio of the active power (P) by the apparent power (S):

$$PF = \frac{P}{S} \times 100\%, \quad (2)$$

where it is commonly expressed as percentage.

The active power (P) is defined by (3) as the average of voltage (v) times current (i) within a predefined number of samples (N):

$$P = \sum_{j=0}^{N-1} \frac{v_j \cdot i_j}{N}, \quad (3)$$

The apparent power (S) as stated by

$$S = V_{RMS} \cdot I_{RMS}, \quad (4)$$

is calculated by the multiplication of the effective values for voltage and current.

To calculate the harmonic distortion it is required to compute discrete Fourier transform (DFT) to obtain the signal spectrum in order to get the total harmonic distortion (THD) index, as stated by

$$THD = \sqrt{\sum_{h=1}^{\infty} P_h}, \quad (5)$$

where P_1 is the power of the fundamental frequency and P_h are the harmonics and interharmonics power, depending if the h takes integer or fractional values respectively.

In a three phases system, to simplify the overall voltage phases presentation a total RMS (TRMS) is used as defined by

$$V_{TRMS} = \frac{1}{3} \sqrt{V_{RMS,A}^2 + V_{RMS,B}^2 + V_{RMS,C}^2}, \quad (6)$$

where $V_{RMS,A}$ represents the phase A and so on. The I_{TRMS} is calculated in a similar way than the V_{RMS} . In addition, to provide an estimation of the voltage imbalance between two phases, a normalized value is computed as stated by

$$UF = \frac{(\Delta V_{RMS})}{V_{nom}} \times 100\%, \quad (7)$$

where ΔV_{RMS} represents the difference between two effective voltage values among phases, and V_{nom} represents the nominal line value.

In order to detect PQD and compute power consumption, some calculations must be done on-line by the smart meter; while some others require an off-line approach such as disturbance propagation. Thus, the smart sensor network needs to perform some calculations in situ and others with the help of a big-data post processor.

3. Smart sensor network architecture

The proposed smart sensor network is based on smart sensors that can be installed on a non-intrusive way inside a wide variety of buildings, such as residential homes, industrial facilities or public buildings. This smart sensor is based on the FPGA technology; it integrates a data acquisition module, a massive storage device, and wireless Bluetooth communication module. Additionally, it internally implements a microprocessor, a real time clock, a universal serial bus (USB), an internal data bus, and several signal processing soft-cores. In order to integrate the smart sensor network, the system utilizes a mobile device such a smartphone or tablet, this device is used to synchronize smart sensors and to monitor them remotely. The system produces a large amount of data that are post processed in a big-data center. Fig. 1 depicts a general system architecture showing the main components in the proposed smart sensor network. This system is very easy to use because the smart sensors are non-intrusive; it allows connecting them without

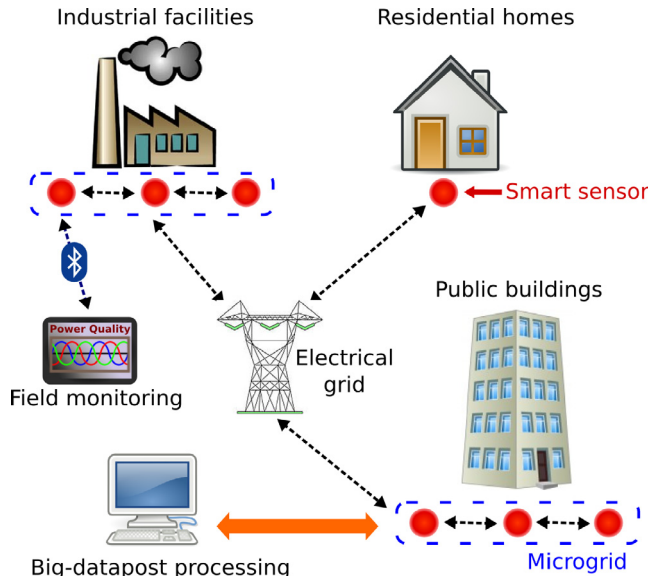


Fig. 1. Overall smart sensor network architecture.

interrupting the energy supply. In addition, it is very flexible because it supports several current and voltage ranges and many customizable processing functions based on soft-cores. Fig. 2 shows a functional block diagram of the developed smart sensor.

Data acquisition of electrical variables is done through a series of stages; since current and voltage are sampled by the same device, it must be well conditioned. Firstly, an impedance coupling stage receives the current and voltage probes; the current probes are inductive elements that typically require input impedance above $10\text{ k}\Omega$, whereas voltage probes require impedance above $250\text{ k}\Omega$. In both cases the signal must be in the range of $\pm 2\text{ VDC}$. Secondly, an isolation stage is required to decouple physical grounds and to avoid security risks; in this stage an isolation amplifier is used and it provides a differential amplification gain of 8. Thirdly, a filtering stage is needed to avoid signal aliasing; this stage is implemented as a passive low-pass filter with a cutoff frequency of 20% below the half of the sampling frequency. Finally, the signals are within the range of the 8-channel analog-to-

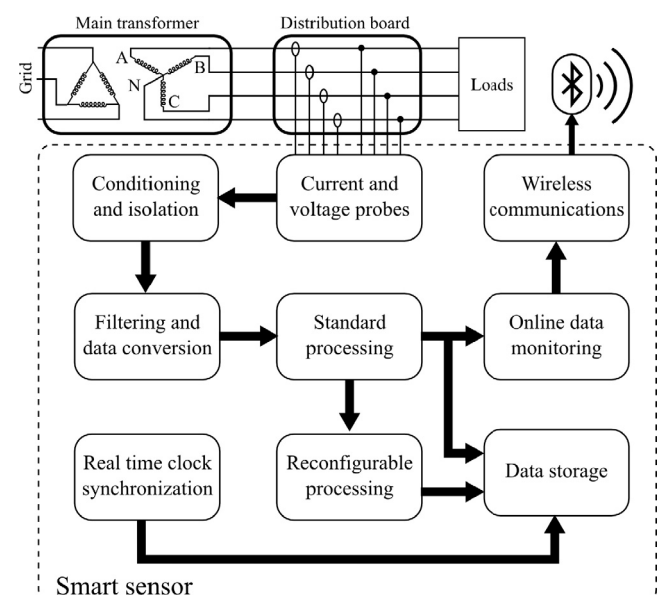


Fig. 2. Functional diagram of the proposed smart meter.

digital converter (ADC); the selected ADC includes a programmable gain amplifier (PGA) and an electromagnetic interference (EMI) filter specially designed for PQ applications. This ADC has a maximum sampling rate of 8000 samples per second, per channel. The FPGA is responsible for the ADC control, to configure it properly and to operate it in the proper gain range.

Data processing is performed by the embedded system in the FPGA; their backbone is formed by an embedded proprietary processor, a memory management unit, and an internal data bus. The proprietary processor is a reduced instruction-set computer (RISC) 16-bit processor with modified-Harvard architecture, able to perform one instruction per clock cycle. The memory system is integrated by two internal caches, one for instructions and the other for data; a main external static random access memory (SRAM) and a high capacity non-volatile NAND-NAND flash memory to store program and user data. In addition, a direct memory access (DMA) unit yields a fast data transfer between memory and peripherals.

In order to synchronize data the system has a real time clock (RTC) with a resolution of 1 ms. This RTC should be adjusted when the equipment is installed via the mobile device. The RTC has an accuracy based on the digital system clock that typically has an accuracy of 100 ppm.

The reconfigurable processing is based on soft-cores elements that the user can select depending on the application; for instance, in an industrial environment a harmonic and PQD detectors are preferred, while in a public building the energy consumption is the main concern. Therefore, the user can select the desired processing units according to its necessities and reconfigure the device.

As a smart sensor the system requires various communication channels, this system includes a wired USB for programming and a wireless Bluetooth for operation. Since the equipment is intended to be used in a microgrid, a short range protocol for wireless communications is selected; for future integration in a smart grid, a WiFi module will replace the Bluetooth.

The proposed equipment is able to record the raw current and voltage signals in addition to the processed data, thus it produces a large amount of data; those data are stored in an high capacity external micro-SD memory. As a raw estimation, each measurement unit produces 12 GB of data per day; the system must compress those data; even though the compression, the final size per day is around 6.5 GB. Therefore, for long monitoring periods the SD card should be continuously replaced.

As aforementioned, the system produces a massive amount of data that are partially processed by the equipment, but to analyze an electrical network is necessary to integrate all the individual measurements onto a network image; thus, a post processing stage is required to gather all data and perform integrated analysis to detect events interaction.

4. Smart sensor network test scenarios

In this section, three scenarios are presented to demonstrate the full functionality of the developed smart sensor network. The first scenario presents a residential home monitoring focused on electrical disturbances events, in order to identify appliance cycles, possibly estimating the power consumption per equipment; in this case only one smart sensor is used. The second scenario presents an industrial installation of a building, in this case a smart sensor is installed to monitor power lines to analyze power factor and THD. Finally, the third scenario is a public hospital, where high power equipment shares electrical lines with highly sensitive electromedical equipment; in this case four pieces of equipment were installed in order to make an overall electrical system evaluation.

5. Experimental setup

The presented smart sensor is based on a Xilinx® FPGA Spartan6 (XC6SLX16) and a 16-bit analog-to-digital converter with 8 channels from Texas Instruments® (ADS130E08) delivering up to 8000 samples per second, per channel. The voltage signal is acquired by a resistive divisor between each phase and neutral; meanwhile, current is acquired by commercial current clamps: Fluke® i200, Fluke® i400, and Fluke® i3000s-FLEX. Both, voltage and current have galvanic isolation from the measurement system by isolation amplifiers. The presented smart sensor is a non-intrusive equipment since it is not necessary to suspend the energy flow during installation, uninstallation, nor operation (see Fig. 3).

5.1. First scenario: Residential home

For this case of study a smart meter is connected to the main distribution board in a residential home, as shown in Fig. 4. The electrical installation of the house has two power line phases of 120 VAC at 60 Hz with two 20 A thermomagnetic circuit breaker each. This experiment consists on a 24 h monitoring, processing and recording the two phase voltages and currents waveforms; also, an appliance log is taken to correlate waveforms and appliance behavior. Additionally, the system searches for PQD in the power supply.

5.2. Second scenario: Industrial area

This scenario consist in monitoring a service area in a public building, it includes elevators, air-conditioning, heating, induction motors, welding machines, lighting, offices, vending machines, etc. The electrical installation has three phases and a neutral, 220 VAC at 50 Hz. The installation has passive PF correction equipment. The smart sensor monitors the three voltage phases and the four currents (including neutral) for a period of 24 h. Because the installation extension and the complexity of the whole system, an event log is not feasible; however, PQ indexes such PF and THD are important to evaluate the overall system performance (see Fig. 5).

5.3. Third scenario: Public hospital

The last experiment is conducted in a hospital, where a group of smart sensors are installed along four levels covering one distribution line. The hospital has two main transformers (220 VAC at

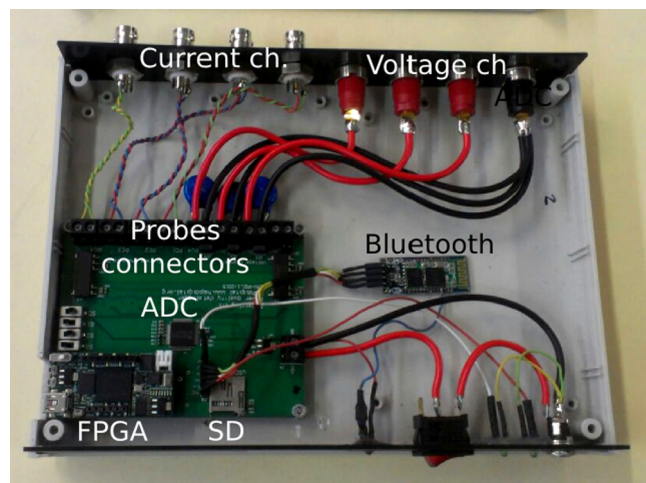


Fig. 3. Developed smart meter showing its internal components.

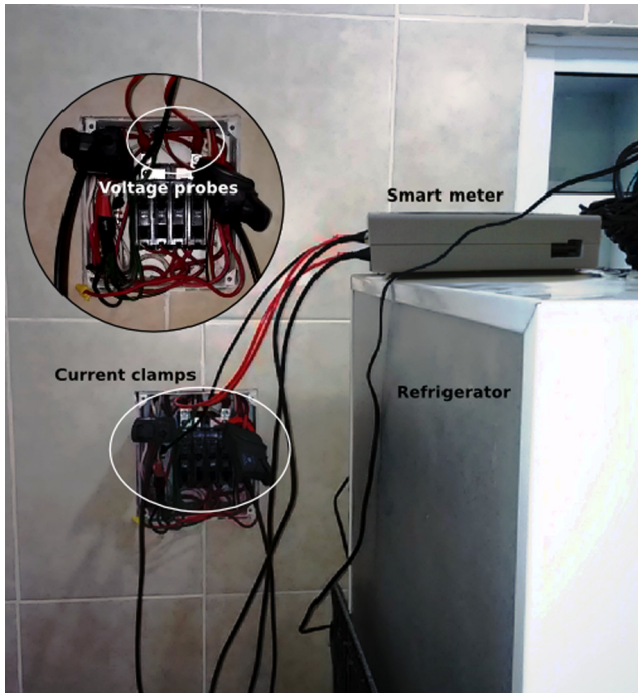


Fig. 4. Smart sensor installed in a residential home at the main distribution board behind the refrigerator in the kitchen.

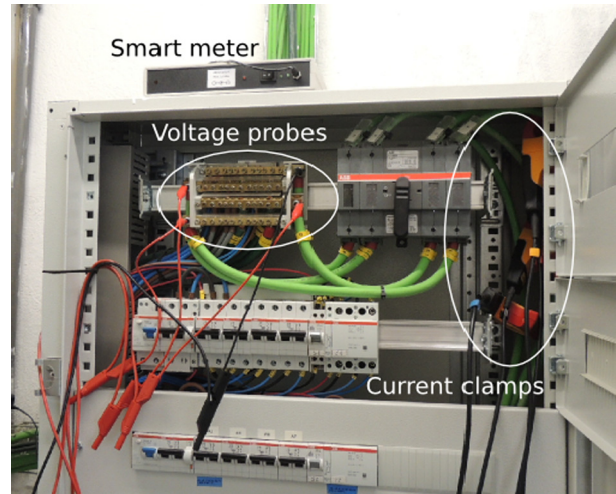


Fig. 6. Smart sensor installed in a secondary distribution board at the hospital facility.

accurate synchronization, the smart sensor network is capable of detecting events to correlate them in different points of the electrical installation. The experiment consists on a week of monitoring for the three voltage phases and the four currents at the different building levels.

6. Results and discussion

The three mentioned scenarios demonstrate the different capabilities of the developed smart sensor network, such as real-time processing, synchronization, and big-data handling among others.

6.1. First scenario: Residential home

This section presents the results of 24 h NILM in a residential home. Fig. 7 shows the RMS voltage of each phase, where RMS is computed each minute, whereas the nominal RMS voltage is 120 VAC; thus, the monitored voltage is slightly over the nominal value but within the 10% of tolerance stated by the norm EN50160 [5] before being considered as a voltage swell. However, there is a small imbalance between both voltage phases that corresponds to the 0.64% of nominal voltage, computed by (7).

While in Fig. 7 both phases behave in a similar way, currents in Fig. 8 have very different behavior, in this case the load interaction is evident. The RMS current is computed within a minute stamp. Fig. 8 shows several interest points; at first glance the phases A and B are fairly independent, mainly because in the A-phase house corresponds to the top level and B phase corresponds to the bottom level. At the bottom level, common areas such kitchen, hall, TV room, diner hall, etc., are located. At the top level are the bedrooms, bathrooms and a balcony. The current monitoring allows identifying the loads connected to the supply line that are also compared with the events log. Therefore, the interest point marked as 1 in Fig. 8 located at 14:00 in the Ib current corresponds to a cyclic consumption load that turns on and off in periods of approximately 40 min, this load resembles the refrigerator behavior; moreover, reviewing the event log this is confirmed. The point 2 in Fig. 8 corresponds to two high peaks of short duration; these peaks match with the microwave oven operation in the event log, those peaks are highly recognizable near to the 18:00, 00:00 and 13:00, during meal time. A zoom at the point 2 of Fig. 8 is presented in Fig. 9a where the interaction in both phases is evident. This interaction is produced by the microwave oven, where the

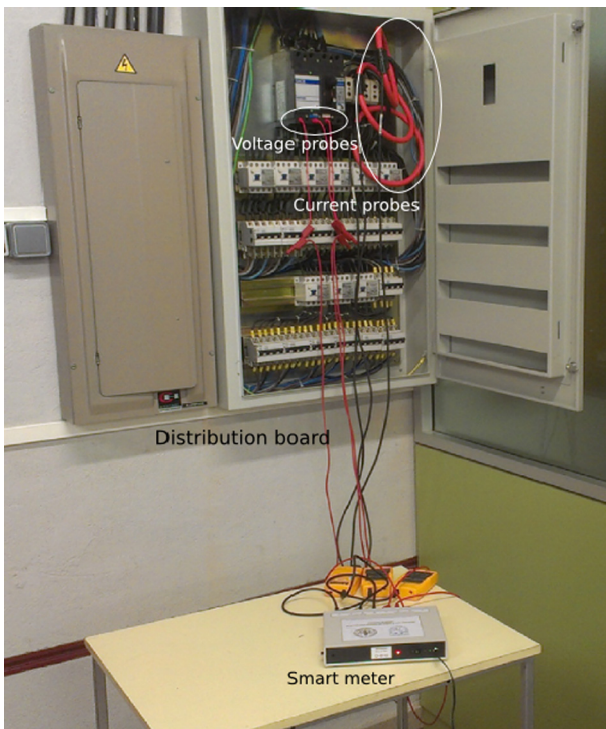


Fig. 5. Smart sensor installed in an industrial area at the main distribution board.

50 Hz) that are connected to a main distribution board, then the installation is divided into general distribution boards (GDB) and this in secondary distribution boards (SDB). Every GDB covers a building block of approximate 6,400 m², and every SDB covers an approximate of 420 m², Fig. 6 shows a smart sensor installation in a secondary distribution board. In this scenario the synchronization of the smart sensor network is an essential issue. Having an

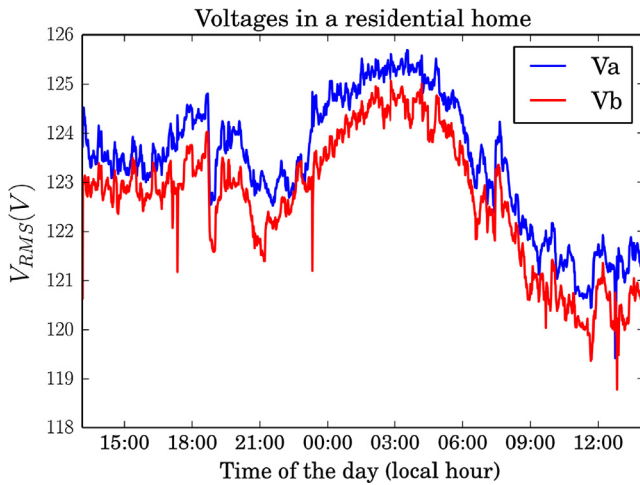


Fig. 7. One-day RMS monitoring for the residential home scenario with two voltage phases.

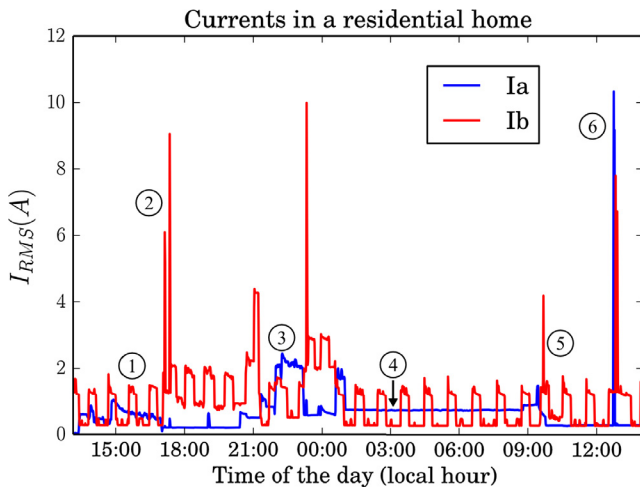


Fig. 8. Currents for the two phases in the residential home monitoring of 24 h.

high peaks occurs in phase B and they are also detected in the phase A. This could be due to an electromagnetic interference effect or due to a signal reflection at the transformer.

The point 3 in Fig. 8 corresponds to the Ia signal and belongs to the TV in a bedroom according to the events log. The point 4 corresponds to the exterior night lights which turns on at midnight and turns off at 10:00. The point 5 corresponds to the signal Ib, a zoom area is presented in Fig. 9b, this it is not only an image enlargement, the smart sensor recalculates the RMS value with higher resolution, in this case one sample per minute; this point marks a small disturbance in the Ib signal over the fridge cycle, this signal corresponds to the blender in the kitchen. Finally, point 6 of Fig. 8 indicates the high peak in the Ia signal that corresponds to a hot-air hair dryer. Therefore, the presented smart sensor allows tracking individual appliances to find out its own power consumption; moreover, with a deeper analysis it will be possible to detect failures or problems in the electrical system.

Another test carried out in this experiment is the PQD detection. In this test, two disturbances were found, one voltage dip and one short interruption, as shown in Fig. 10. The interruption shown in Fig. 10a the voltage in both phases drops below 1% of the nominal voltage with duration of 504 ms, happens at 13:09:09 with an offset of 200 ms from the stated time. Meanwhile, the voltage dip has duration of five cycles (aprox. 80 ms) as shown in Fig. 10b, the

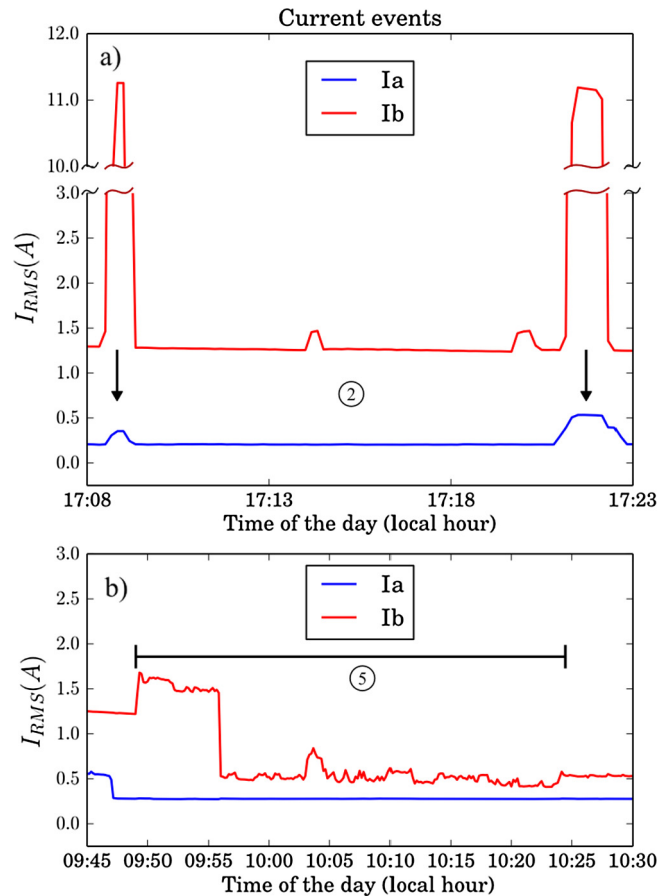


Fig. 9. (a) Interaction between phases because the high consumption peak due to the microwave oven, (b) High frequency signal injected by blender activation.

voltage amplitude drops below the 78% of the nominal line voltage at 13:22:10 with a time offset of 260 ms. This test demonstrates the ability of the proposed smart sensor to detect real PQD events.

6.2. Second scenario: Industrial area

The second experiment tests the smart sensor in a different scenario, in this case an industrial installation that powers elevators, heating, venting, lighting, wall outlets, among others. Additionally, the electrical system includes especial equipment to correct the power factor. The 24 h monitoring in the 220 VAC installation, shown in Fig. 11 where V_{RMS} values are computed by (1); gives a waveform almost identical in the three voltage phases, as expected. Yet, the voltages are above the nominal line value but it is not enough to be considered as a voltage swell. However, the average unbalance for the three phases is 0.24% with respect to the nominal voltage of 220 VAC.

In the current signal shown in Fig. 12, it is evident the difference in all monitored phases. The phase Ia is mainly connected to wall outlets that powers office equipment such as PCs, printers, photocopiers, etc. The Ia phase is clearly active at working hours from 8:00 to 19:00 with a recess for the meal time at around 15:00. Points 2 and 5 of Fig. 12a mark the high activity moments. Meanwhile, the Ib phase drives the heating and venting system in the building, leading it to the highest current flow with many transient episodes. Those transients could be due to the fan motors startup in the venting system, as shown in Fig. 12a mark 1; in addition, the current is higher at night, because the test was performed in winter season. The Ic phase current has the steadiest flow, this

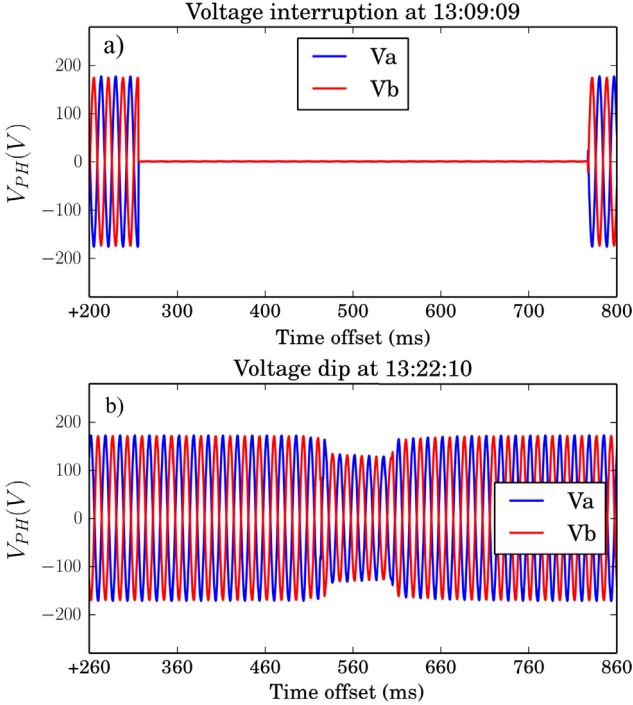


Fig. 10. Voltage per phase (V_{PH}) signal of found disturbances in the residential scenario: (a) voltage dip event detected by the smart sensor, (b) voltage interruption event detected by the smart in the residential home scenario.

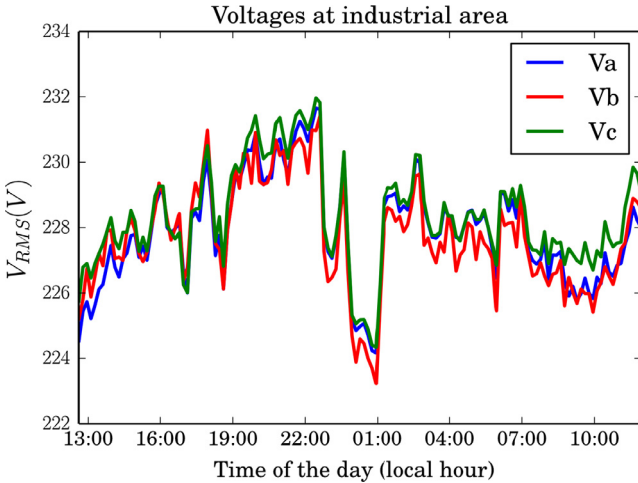


Fig. 11. One day voltage monitoring in the industrial area scenario with three phases, the alternating voltage signal is expressed in root mean square (RMS) values.

phase corresponds to the lighting system, elevators and some vending machines, mark 3 of Fig. 12c. For the night period marked as point 4 the current consumption is minimum for phase A, it is almost steady for phase C, and cyclic for phase B, which is the expected behavior. It is evident that the three phases are used as separated lines, this is clearly an unbalanced system that produces high neutral currents with an average of 7 A, as shown in Fig. 13.

In order to evaluate the equipment for power factor correction, the smart sensor computes power factor from the measurements according to the EN50160 norm in periods of 10 min, shown in first column of Fig. 14. It is clear that for phases B and C the PF compensation is working well, but for phase A there are three events (marks 1, 2, and 4) where the PF goes below the 0.9 which is the

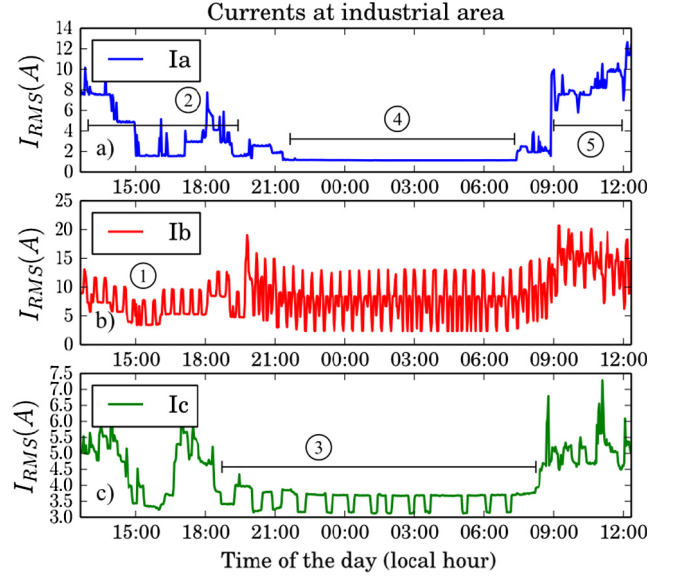


Fig. 12. One day current monitoring in the industrial area scenario with three phases expressed in root mean square current (I_{RMS}). (a) phase A mainly connected to office equipment, (b) phase B mainly connected to heating and venting system, (c) phase C mainly connected to lighting and elevators.

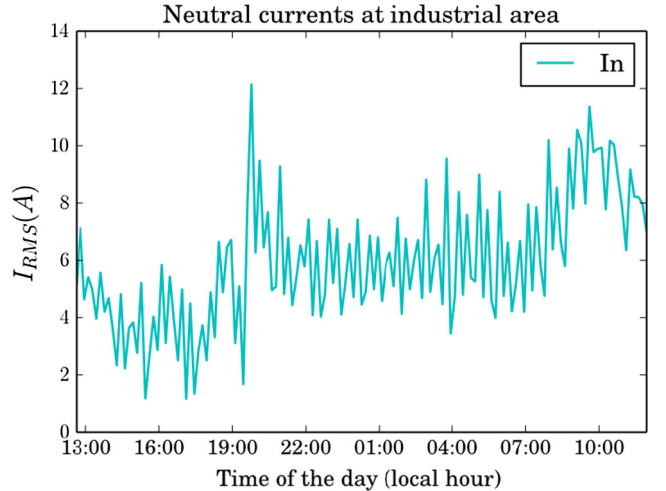


Fig. 13. Neutral current in the industrial area scenario.

limit according to the applicable regulations. This low PF happens in the phase with lower consumption, but is where the most of loads are electronic equipment that contains switching power supplies that pollutes the line with many harmonics which are not properly filtered by the PF compensation equipment.

To corroborate the presence of harmonic components a THD is computed for voltage signal shown in the second column of Fig. 14, and for current signal shown in Fig. 14 third column. The harmonics components for the three voltage phases are computed and it is found that the THD during the whole monitoring period is below 5% which is within the permissible limits by the applicable regulations. Furthermore, because the current depends on the load demand, the computed THD high as result of connection and disconnection of loads, as shown in third column of Fig. 14. Moreover, phases Ib and Ic have little variations meanwhile Ia varies in a broad range, Fig. 14c. This wide variation onto Ia comes as a result of the connection of plenty switching supplies operating that heavily distorts the ideal sinusoidal waveform. In Fig. 14c the current

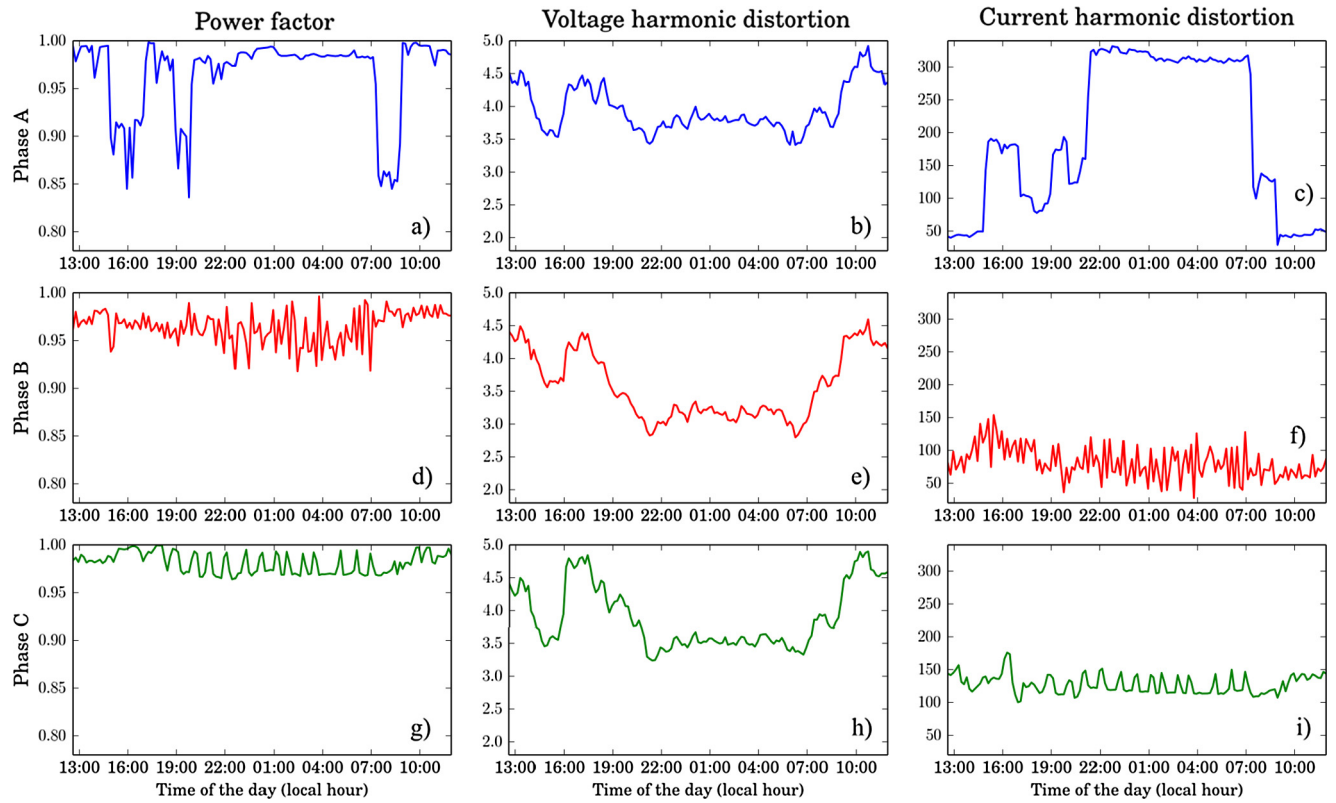


Fig. 14. Power factor and total harmonic distortion per phase during 24 h monitoring in an industrial area, (a) PF in phase A, (b) Voltage THD in phase A, (c) Current THD in phase A, (d) PF in phase B, (e) Voltage THD in phase B, (f) Current THD in phase B, (g) PF in phase C, (h) Voltage THD in phase C, and (i) Current THD in phase C.

THD increases because the consumption is very low at night; hence, the noise present in the line produces a rise of the THD.

6.3. Third scenario: Smart sensor network

The last scenario demonstrates the use of the developed smart sensor network. In this scenario four smart sensors are installed in a public hospital facility, covering the sector 3 of the power distribution line depicted in Fig. 15. The smart sensors are installed at the main distribution board (CG-3), this board have fourteen secondary distribution boards, from them were selected three boards (CS-301, CS-311, and CS-312) covering different operation conditions. The CS-301 is connected to the lighting of one storage room and some stairs; it is assumed that the current consumption in this area will be low. The board CS-311 is connected to one nurses station and some halls, the electrical equipment connected to this

board consists mainly in computers, vending machines, lighting, microwave ovens, coffee makers, and water dispensers; thus, it is expected a moderate consumption with episodes of high flow due to microwave ovens. Finally, the CS-312 is used in the X-ray area and in some consulting rooms; a high current consumption is expected due to the X-ray equipment.

In order to present a comprehensible analysis about the monitoring, a TRMS is computed according to (6) to obtain a single value per monitored board in voltage and a single value for currents in the three line phases. The monitoring period at the hospital is one week; however, in order to accurately appreciate the system behavior the results show the second day of monitoring that corresponds to December 2nd of 2015. As shown in Fig. 16, the voltages at the four monitoring points behave in a very similar way. Where the changes in TRMS are synchronized, it is the expected behavior because the voltage in the entire installation theoretically should be the same; however, there are certain voltage offset between monitoring boards. At this point, it is unknown what produces those offsets but probably are a result of the neutral cable length and the high neutral currents, shown in Fig. 17.

It is well known that neutral currents take place because unbalanced loads, since the installation have mainly single phase equipment it is expected to observe high neutral currents, see Fig. 17. In boards CS-301 and CS-311 the imbalance is fairly constant in all day. For CS-312 the imbalance rises at 8:00 with many fluctuations, since the X-ray equipment uses only one phase it produces a high phase unbalance, reflected as a high neutral current. In the CG-3 board is observed the general imbalance for the entire branch, which is close to 8 A of average current in the whole day.

In contrast with the voltages at monitoring points which behaves in a close way, the currents shown in Fig. 18 have a dissimilar behavior. In Fig. 18a the general board shows an overall increment in the current flow (point 2) at the working hours from

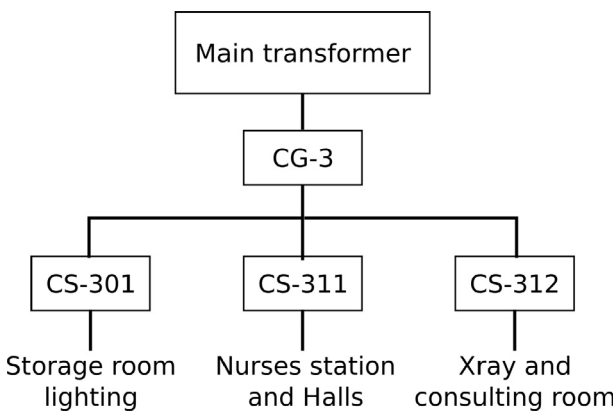


Fig. 15. Diagram of the installed smart sensor network and its corresponding uses.

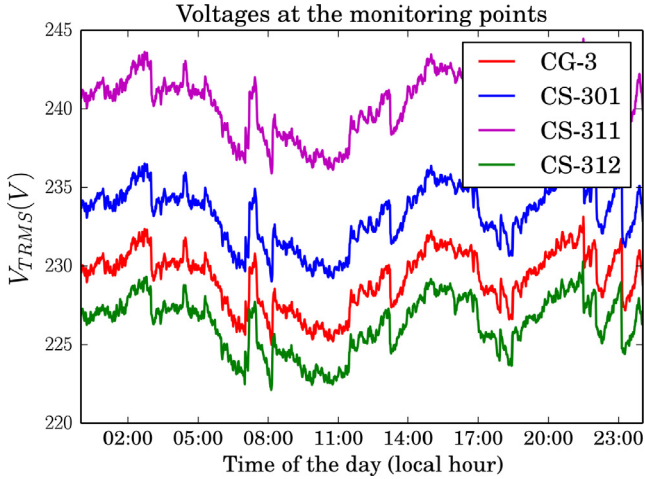


Fig. 16. Total RMS voltages (V_{TRMS}) per monitoring smart sensor in the network.

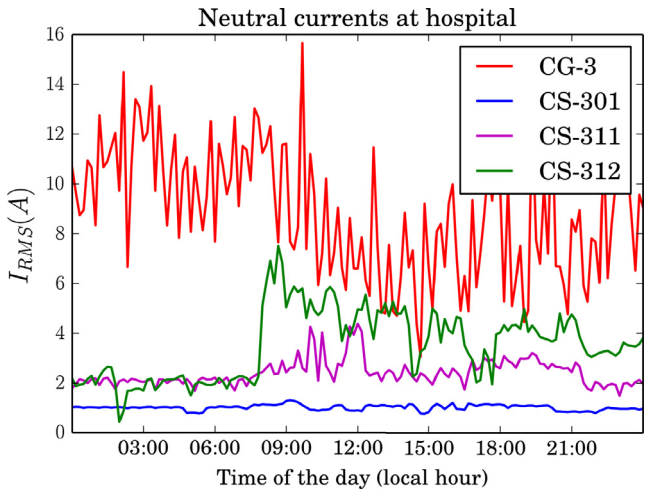


Fig. 17. Total RMS neutral currents per monitoring smart sensor in the network.

8:00 to 21:00, at night the current keeps around 60 A for the whole installation. The CS-301 board consumes very little current, around 600 mA, as was expected because this board provides energy to light a storage room and some stairs that are scarcely used. The smart sensor is located at the board CS-301 to test its performance with small signals, as it can be seen in Fig. 18b at day hours from 10:00 to 16:00 the current drops almost to zero, because the lights turns off in favor of natural light in the stairs; at night hours, the current is fairly constant because the stair light stays on. The CS-311 presents the most active line in Fig. 18c, this smart sensor detects several interesting points to discuss. First, the point marked as 1 in Fig. 18c resembles the refrigerator cycle in the residential home scenario, at the time of smart sensor installation it was noted that some halls have vending machines with products that needs refrigeration; thus the found signal can be attributable to refrigerated vending machines. Moreover, the mark 4 in Fig. 18c corresponds to those highly recognizable peaks produced by the microwave ovens, by observing the time when those peaks happen, it is found that they correspond to lunch time. Besides, those peaks are only present at working hours. Another remark is the offset present at night hours, this offset can be attributed to lighting, resembling the previous comments on CS-301, the offset almost disappears when natural light is available, at night the offset returns to its previous level of 3 A. The last equipment located at CS-312 board shows a different behavior from the others sec-

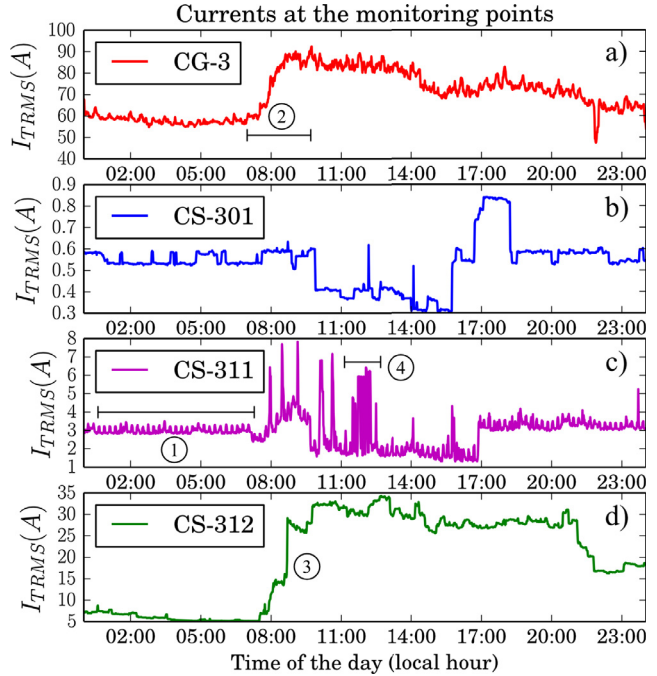


Fig. 18. Total RMS currents per monitoring smart sensor in the network: (a) general distribution board, (b) secondary board CS-301, (c) secondary board CS-311, and (d) secondary board CS-312.

ondary boards, since this distribution board has a very specific task. It is noticed that at mark 3 of Fig. 18d a high current consumption appears by the activation of the X-ray equipment. Therefore, looking at the Fig. 17, it is evident that the neutral current on CS-312 gets larger; thus, these two effects can be correlated with the operation of the X-ray equipment. Yet, the current signal indicates the presence of some other equipment that could not be identified that with a deeper analysis its identification is feasible.

The three scenarios presented demonstrate some features of the proposed smart sensor network, not only to perform measurements based on normative, but it also to allow to correlate events at the same monitoring point as well in several remote points that shares the same line.

7. Conclusion

This work presents a smart sensor network that allows inspecting an electrical installation in a non-intrusive way. It delivers standard measurements but it is not limited to them, it also allows examining: PQD events in detail, interactions between lines, identify electrical equipment, correlate events between monitoring points, among others. Furthermore, the presented smart sensor network is a powerful tool to evaluate an electrical system which potentially can detect failures in the system; in order to reach that detail level further research shall be performed. This proposed smart sensor network with its real-time calculations capacities and the big-data support in the network have promising interesting applications in the future smart grid. Further work will include the analysis of renewable energy facilities such solar and wind power plants in order to detect power losses in the energy supply system.

Funding

This work was supported by SEP-CONACyT [222453-2013]; the FOMIX [QRO-2014-C03-250269]; and the Autonomous University of Queretaro [FOFIUAQ-FIN201613].

Acknowledgments

The authors wish to thank the Universidad de Valladolid, Sindicado de Castilla y León (SACyL), and Rio Hortega hospital, Spain, for allowing using their facilities for this research.

References

- [1] M. Jaradat, M. Jarrah, A. Bousselham, Y. Jararweh, M. Al-Ayyoub, The internet of energy: smart sensor networks and big data management for smart grid, *Procedia Comput. Sci.* 56 (2015) 592–597, <http://dx.doi.org/10.1016/j.procs.2015.07.250>.
- [2] J. Rivera, G. Herrera, M. Chacon, P. Acosta, M. Carrillo, Improved progressive polynomial algorithm for self-adjustment and optimal response in intelligent sensors, *Sensors* 8 (2008) 410–7427, <http://dx.doi.org/10.3390/s8117410>.
- [3] C. Shuxiang, Y. Haiwen, C. Yong, T. Bo, L. Jianxun, An ISO/IEC/IEEE21451 smart sensor network for distributed measurement of pavement structural temperature, *Int. J. Distrib. Sens. Netw.* 2016 (2016) 1–13, <http://dx.doi.org/10.1155/2016/3408489>.
- [4] IEEE Standard, IEEE Std 1159, Recommended Practice for Monitoring Electric Power Quality, IEEE Standard 1159, 1995.
- [5] BSi, EN50160:2010 Voltage Characteristics of Electricity Supplied by Public Distribution Networks, EN50160, 2010.
- [6] IEC, IEC 60364-1 Low-voltage Electrical Installations – Part 1: Fundamental Principles, Assessment of General Characteristics, Definitions, IEC International Standard, 2005.
- [7] IEC, Electrical Installations of Buildings – Requirements for Special Installations or Locations – Medical Locations, IEC International Standard 60364-7-710, 2008.
- [8] IEEE Standard, Recommended Practices for Electric Systems in Health Care Facilities, IEEE Standard 602, 1996.
- [9] S. Khokhar, A. Asuhaimi, B.M. Zin, A.S.B. Mokhtar, M. Pesaran, A comprehensive overview on signal processing and artificial intelligence techniques applications in classification of power quality disturbances, *Renew. Sust. Energy Rev.* 51 (2015) 1650–1663, <http://dx.doi.org/10.1016/j.rser.2015.07.068>.
- [10] A. Elsherif, T. Fetouh, H. Shaaban, Power quality investigation of distribution networks embedded wind turbines, *J. Wind Eng.* 2016 (2016) 1–17, <http://dx.doi.org/10.1155/2016/7820825>.
- [11] K.R. Prakash, K. Nand, R.M. Soumya, Islanding and power quality disturbance detection in grid-connected hybrid power system using wavelet and S-transform, *IEEE Trans. Smart Grid* 3 (2012) 1082–1094, <http://dx.doi.org/10.1109/TSG.2012.2197642>.
- [12] D. Camarena-Martinez, M. Valtierra-Rodriguez, C.A. Perez-Ramirez, J.P. Amezquita-Sanchez, R.J. Romero-Troncoso, A. Garcia-Perez, Novel downsampling empirical mode decomposition approach for power quality analysis, *IEEE Trans. Ind. Electron.* 63 (2016) 2369–2378, <http://dx.doi.org/10.1109/TIE.2015.2506619>.
- [13] O. Prakash Mahela, A. Gafoor Shaik, Topological aspects of power quality improvement techniques: A comprehensive overview, *Renew. Sust. Energy Rev.* 58 (2016) 1129–1142, <http://dx.doi.org/10.1016/j.rser.2015.12.251>.
- [14] D. Kolokotsa, The role of smart grids in the building sector, *Energy Build.* 116 (2016) 703–708, <http://dx.doi.org/10.1016/j.enbuild.2015.12.033>.
- [15] H. Apaydin-Özkan, A new real time home power management system, *Energy Build.* 97 (2015) 56–64, <http://dx.doi.org/10.1016/j.enbuild.2015.03.038>.
- [16] R.J. Cerqueira-Pinto, S.J. Pinto-Simões-Mariano, M.R. Alves-Calado, Power quality experimental analysis on rural home grid-connected PV systems, *Int. J. Photoenergy* 2015 (2015) 1–8, <http://dx.doi.org/10.1155/2015/791680>.
- [17] G. Habash, D. Chapotchkine, P. Fisher, A. Rancourt, R. Habash, W. Norris, Sustainable design of a nearly zero energy building facilitated by a smart microgrid, *J. Renew. Energy* 2014 (2014) 1–11, <http://dx.doi.org/10.1155/2014/725850>.
- [18] N. Christiansen, M. Kaltschmit, F. Dzukowski, F. Isensee, Electricity consumption of medical plug loads in hospital laboratories: Identification, evaluation, prediction and verification, *Energy Build.* 107 (2015) 392–406, <http://dx.doi.org/10.1016/j.enbuild.2015.08.022>.
- [19] D. Capriglione, L. Ferrigno, V. Paciello, A. Pietrosanto, A. Vaccaro, Experimental characterization of consensus protocol for decentralized smart grid metering, *Measurement* 77 (2016) 292–306, <http://dx.doi.org/10.1016/j.measurement.2015.09.024>.
- [20] R. Bayindir, I. Colak, Smart grid technologies and applications, *Renew. Sust. Energ. Rev.* 66 (2016) 499–516, <http://dx.doi.org/10.1016/j.rser.2016.08.002>.
- [21] J. Seo, J. Jin, J.Y. Kim, J.-J. Lee, Automated residential demand response based on advanced metering infrastructure network, *Int. J. Distrib. Sens. Netw.* 2016 (2016) 1–10, <http://dx.doi.org/10.1155/2016/4234806>.
- [22] Fluke Co., Fluke 434-II/435-II/437-II Three Phase Energy and Power Quality Analyzer, Users Manual rev.1 06/12, 2012.
- [23] S.A. Circutor, Power Quality Analyzers K-QNA500, K-QNA500 8IO and K-QNA500 8IOR, User Manual, M98239501-03-16A, 2016.
- [24] Hioki E.E. Co., PW3198 Power Quality Analyzer, Instruction Manual, 2012.
- [25] R. Klis, E.N. Chatzi, Vibration monitoring via spectro-temporal compressive sensing for wireless sensor networks, *Struct. Infractr. E* 13 (1) (2017) 195–209, <http://dx.doi.org/10.1080/15732479.2016.1198395>.
- [26] J.E. Noriega-Linares, J.M. Navarro-Ruiz, On the application of the raspberry pi as an advanced acoustic sensor network for noise monitoring, *Electron.* 5 (4) (2016) 1–14, <http://dx.doi.org/10.3390/electronics5040074>.
- [27] A. Glowacz, Z. Glowacz, Diagnosis of stator faults of the single-phase induction motor using acoustic signals, *Appl. Acoust.* 117 (2017) 20–27, <http://dx.doi.org/10.1016/j.apacoust.2016.10.012>.
- [28] A. Glowacz, Diagnostics of rotor damages of three-phase induction motors using acoustic signals and SMOFS-20-EXPANDED, *Arch. Acoust.* 41 (3) (2016) 507–515, <http://dx.doi.org/10.1515/aoa-2016-0049>.
- [29] A. Glowacz, Z. Glowacz, Diagnosis of the three-phase induction motor using thermal imaging, *Infrared Phys. Techn.* 81 (2017) 7–16, <http://dx.doi.org/10.1016/j.infrared.2016.12.003>.
- [30] E. Guillen-Garcia, A.L. Zorita-Lamadrid, O. Duque-Perez, L. Morales-Velazquez, R.A. Osornio-Rios, R.J. Romero-Troncoso, Power consumption analysis of electrical installations at healthcare facility, *Energies* 10 (1) (2017) 1–14, <http://dx.doi.org/10.3390/en10010064>.